A&A 617, A56 (2018)
https://doi.org/10.1051/0004-6361/201833548

Astronomy & Astrophysics

A CEMP-no star in the ultra-faint dwarf galaxy Pisces II⋆

M. Spite[1], F. Spite[1], P. François[1,2], P. Bonifacio[1], E. Caffau[1], and S. Salvadori[1,3,4]

[1] Observatoire de Paris, PSL University, CNRS, GEPI, Place Jules Janssen, 92195 Meudon, France
e-mail: monique.spite@obspm.fr
[2] Université de Picardie Jules Verne, 33 rue St-Leu, 80080 Amiens, France
[3] Dipartimento di Fisica e Astronomia, Universitá di Firenze, Via G. Sansone 1, Sesto Fiorentino, Italy
[4] INAF/Osservatorio Astrofisico di Arcetri, Largo E. Fermi 5, Firenze, Italy

Received 1 June 2018 / Accepted 20 June 2018

ABSTRACT

Aims. A probable carbon enhanced metal-poor (CEMP) star, Pisces II 10694, was discovered recently in the ultra-faint (UFD) galaxy Pisces II. This galaxy is supposed to be very old, suspected to include dark matter, and likely formed the bulk of its stars before the reionisation of the Universe.
Methods. New abundances have been obtained from observations of Pisces II 10694 at the Kueyen ESO VLT telescope, using the high-efficiency spectrograph: X-shooter.
Results. We found that Pisces II 10694 is a CEMP-no star with [Fe/H] = −2.60 dex. Careful measurements of the CH and C_2 bands confirm the enhancement of the C abundance ([C/Fe] = +1.23). This cool giant has very probably undergone extra mixing and thus its original C abundance could be even higher. Nitrogen, O, Na, and Mg are also strongly enhanced, but from Ca to Ni the ratios [X/Fe] are similar to those observed in classical very metal-poor stars. With its low Ba abundance ([Ba/Fe] = −1.10 dex) Pisces II 10694 is a CEMP-no star. No variation in the radial velocity could be detected between 2015 and 2017. The pattern of the elements has a shape similar to the pattern found in galactic CEMP-no stars like CS 22949-037 ([Fe/H] = −4.0) or SDSS J1349+1407 ([Fe/H] = −3.6).
Conclusions. The existence of a CEMP-no star in the UFD galaxy Pisc II suggests that this small galaxy likely hosted zero-metallicity stars. This is consistent with theoretical predictions of cosmological models supporting the idea that UFD galaxies are the living fossils of the first star-forming systems.

Key words. stars: abundances – Local Group – galaxies: dwarf – galaxies: abundances

1. Introduction

The ultra-faint dwarf (UFD) galaxies contain the largest fraction of metal-poor stars of any galaxy type (e.g. Kirby et al. 2008) and they could be the direct descendants of the first generation of galaxies in the Universe (Bovill & Ricotti 2009; Salvadori & Ferrara 2009). It has been shown that the chemical composition of the UFD stars is very similar to the chemical composition of the extremely metal-poor (EMP) galactic stars, (see e.g. François et al. 2016; Ji et al. 2016a,b).

In our Galaxy, in the "normal" EMP turn-off stars, the abundance ratios of the elements with respect to Fe is about the same as that found in solar-type stars, except for the α elements which are slightly enhanced with respect to iron (e.g. [Ca/Fe] ≈ 0.3 dex). In these stars, C is also slightly enhanced: [C/Fe] has been found equal to 0.45 ± 0.10 (Bonifacio et al. 2009). Many giants undergo a deep mixing that transforms the atmospheric carbon into nitrogen, and consequently their carbon abundance is systematically lowered relative to turn-off stars, sometimes with [C/Fe] < 0. The abundance of the elements heavier than Zn (neutron-capture elements) is very scattered in the classical EMP turn-off and giant stars (François et al. 2007; Spite et al. 2018).

At low metallicity many stars are carbon-enhanced compared to the normal EMP stars. If we sample stars of lower and lower metallicity, we find larger and larger fractions of carbon-enhanced stars. About 30% to 40% of the EMP stars with [Fe/H] ≈ −3 possess significant overabundances of carbon relative to iron. This fraction rises to at least 80% for stars with [Fe/H] < −4.0 (Beers 2018), and among the twelve known stars with 60 000 times less metals than the Sun ([Fe/H] < −4.5), only one star (Caffau et al. 2011a; Bonifacio et al. 2015) has a confirmed carbon abundance not compatible with the definition of the CEMP stars adopted here: [C/Fe] > +1.0 (Beers & Christlieb 2005).

The carbon-enhanced metal-poor (CEMP) stars have been extensively studied in our Galaxy at low and high resolution (e.g. Allen et al. 2012; Lee et al. 2013, 2014; Hansen et al. 2016; Yoon et al. 2016, and references therein). They are characterised by a strong overabundance of carbon, and very often an overabundance of nitrogen, oxygen, and magnesium. Moreover, they have very diverse abundances of the neutron-capture elements: some are very strongly polluted by neutron-capture elements built by the slow ("s") and sometimes the rapid ("r") processes (here we call all of them CEMP-s). Others CEMP stars do not show any enhancement of the neutron-capture elements compared to the normal metal-poor stars and they are called "CEMP-no". In our Galaxy, all the most metal-poor carbon-rich stars ([Fe/H] < −3.6) belong, as far as we know, to the group of the CEMP-no (Spite et al. 2013; Bonifacio et al. 2015; Caffau et al. 2018): their carbon abondance A(C) is always between A(C) = 5.5 and 7.7. At higher metallicity some stars are CEMP-no, but most of them are CEMP-s: their carbon

⋆ Based on observations collected at the European Organisation for Astronomical Research in the Southern Hemisphere under ESO programme 099.B-0062(A).

abundance can reach A(C) = 8.7, their Ba abundance is very high, and they have generally been found to be binary stars (see e.g. Caffau et al. 2018). According to several authors (e.g. Masseron et al. 2010; Abate et al. 2015), their chemical pattern suggests a previous mass-transfer from their companion in its asymptotic giant branch (AGB) phase.

Since their discovery it has been proposed that the CEMP-no stars formed in an environment polluted by the first stellar generations (e.g. Bonifacio et al. 2003; Nomoto et al. 2003). This idea has been further confirmed by several authors who suggest that the carbon in the CEMP-no stars was brought by faint supernovae of zero metallicity (Cooke & Madau 2014; de Bennassuti et al. 2014; Bonifacio et al. 2015). Probably the C-enhancement made it easier for them to form from a gas depleted in other metals, and the large scatter of the carbon abundance displayed in these stars (about 1 dex) is the result of the nucleosynthesis of a limited number of faint supernovae of zero metallicity that have polluted the gas. If this scenario is correct, then many CEMP-no stars should be also found in dwarf galaxies, and especially in UFD galaxies, which are the faintest ($L < 10^5\ L_\odot$), the more metal-poor, and likely the oldest galactic systems (Salvadori et al. 2015). In recent years, many metal-poor stars have been observed and analysed in the dwarf galaxies of the Local Group, and several teams have been looking for carbon-rich stars (e.g. Norris et al. 2010a; Lai et al. 2011; Frebel et al. 2014, 2016; Skúladóttir et al. 2015; Chiti et al. 2018). To date, however, only five true CEMP stars ([Fe/H] ≤ −2.5 and [C/Fe] > +1) have been observed in these faint systems. All these stars are CEMP-no.

Recently Kirby et al. (2015) have observed spectroscopically seven stars in the UFD galaxy Pisces II ($L = 10^4\ L_\odot$), discovered by Belokurov et al. (2010); however, he was able to measure the metallicity of only four of them. Among these four stars, one, Pisces II 10694, is a CEMP star with [Fe/H] = −2.7. In the Ultra Faint Dwarfs very few stars are observable. Establishing that even one of the stars is a CEMP-no star (or a CEMP-s) can provide useful information. The quality of the spectra of Kirby et al. (2015) did not allow him to determine the C abundance (although the C-enhancement is visible from the CN band between 830 nm and 840 nm) or the abundance of any element other than iron. This star is a cool giant, and thus the probability that it has undergone deep mixing is high. In this case the carbon abundance in the gas that formed the star should have been even higher than observed now in the atmosphere of the star, the abundance of the heavier elements remaining untouched by deep mixing.

The aim of this paper is to determine the abundances of the main elements in Pisces II 10694 from spectra obtained with a higher resolution and in a larger wavelength range than the spectrum studied by Kirby et al. (2015) in order to establish the CEMP type of this star.

2. Observational data

2.1. Spectra and reduction

The g magnitude of Pisces II 10694 is 19.9. This very faint star was observed in service mode with Kueyen (ESO-VLT, UT2) and the high-efficiency spectrograph X-shooter (D´Odorico et al. 2006; Vernet et al. 2011). The observations were performed in staring mode with 1x1 binning and the integral field unit (Guinouard et al. 2006). The stellar light is divided in three arms by X-shooter; we analysed here only the UVB spectra (from 400 to 560 nm with a resolving power $R = 7900$) and the visual (VIS) spectra (from 560 to 1000 nm with $R = 12600$). The signal-to-noise ratio (S/N) of the infrared spectrum ($\lambda > 1000$ nm) is too low to allow the analysis. The spectra were reduced using the same procedure as in Caffau et al. (2013). The total exposure time was 11 h divided in thirteen 3000 s spectra.

Table 1. Radial velocity of Pisces II 10694 measured on the twelve best spectra.

MJD	Geocentric Rad. Vel.	Telluric lines Rad. Vel.	Barycentric correction	Barycentric Rad. Vel.
57934.35	−268.4	−4.4	26.9	−237.1
57955.28	−261.0	−2.2	21.9	−236.9
57955.33	−255.4	−3.4	21.7	−230.3
57956.26	−261.7	−4.0	21.7	−236.0
57963.22	−251.6	0.6	19.3	−232.9
57964.22	−249.7	0.9	18.9	−231.7
57964.31	−252.0	0.8	18.7	−234.1
57965.26	−251.1	3.0	18.5	−235.6
57980.17	−264.2	−15.9	12.5	−235.8
57982.20	−258.2	−13.0	11.5	−233.6
57985.24	−265.1	−16.9	9.9	−238.3
57985.29	−258.8	−15.9	9.8	−233.1

Notes. All the radial velocities are given in km s^{-1}. The barycentric radial velocity is equal to (geocentric Rad. Vel.) − (telluric Rad. Vel.) + (barycentric correction).

2.2. Radial velocities measurements

Thirteen spectra were obtained in 2017 between June 30 and August 20. The radial velocity has only been measured on the twelve spectra with the best S/N (Table 1). The geocentric radial velocity has been established from the position of the H_α line, which is well defined in all the spectra.

Since X-shooter is a single object spectrograph‘ for the Cassegrain focus, it is sensitive to flexures. The flexure correction can be determined from the apparent position of the telluric lines (zero point); for precise measurement of the radial velocity it is very important to take into account this correction.

The uncertainty in the individual measurement of the barycentric radial velocity is less than 4.0 km s^{-1}. From the measurements listed in Table 1 we were not able to detect a variation in the radial velocity between June and August 2017. The mean barycentric radial velocity is -234.6 ± 2.4 km s^{-1}, which is consistent[1] with the value measured on May 2015 (Kirby et al. 2015): -232.0 ± 1.6 km s^{-1}.

3. Abundance analysis

In a first step we interpolated a model in a grid of LTE OSMARCS models (Gustafsson et al. 1975, 2003, 2008) with the atmospheric parameters given by Kirby et al. (2015): $T_{\rm eff} = 4130$ K, $\log g = 0.8$. These parameters are mainly based on photometry and theoretical isochrones from the Yonsei-Yale group (Demarque et al. 2004). With this model we found in

[1] For each star in Pisces, Kirby gives the radial velocity relative to the centre of the Sun (heliocentric radial velocity) neglecting the rotation of the Sun around the gravity centre of the solar system, but the difference between the heliocentric and barycentric velocities is of the order of a few m s^{-1}, which is negligible compared to the measurement errors.

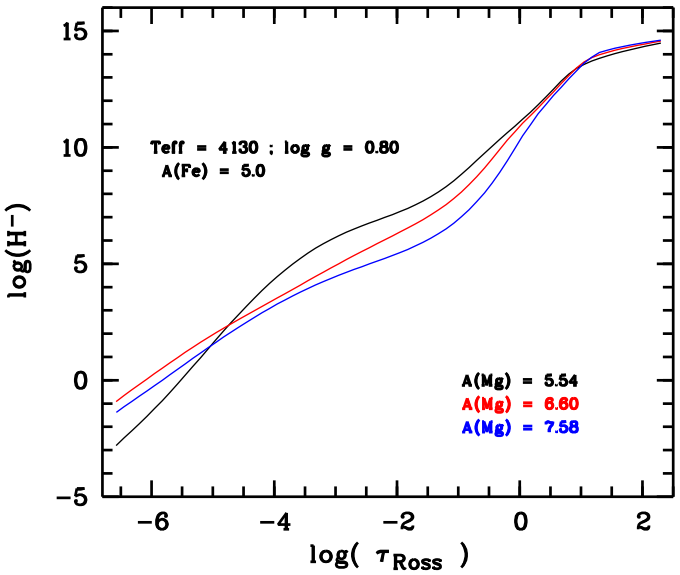

Fig. 1. Number density of H^- vs. optical depth $\log \tau_{Ross}$ for three different abundances of Mg. The blue line (A(Mg) = 7.58) corresponds to the solar abundance of Mg, the red line to the Mg abundance in Pisces II 10694, and the black line (A(Mg) = 5.54) to the Mg abundance expected for a normal metal-poor star with [Fe/H] = −2.6. The molecular bands and the metallic lines are mainly formed between $\log \tau_{Ross} = -2$ and −1, a region where the number density of H^- is strongly affected by the Mg abundance.

Pisces II 10694 a very strong enrichment of C, N, and Mg relative to Fe; our spectrum does not contain Fe II lines, which could constrain the gravity better.

In these cool metal-poor giants, the main source of opacity is the negative hydrogen ion H^- whose abundance depends on the electron density. The main electron donor is always Mg, especially in the atmosphere of Pisces II 10694 since all the other metals are very scarce. As a consequence the continuous absorption strongly depends on the abundance of magnesium. In Fig. 1 we show the influence of the magnesium abundance on the number density of H^-. The metallic lines are formed at an optical depth close to $\log \tau_{Ross} = -1$, and the molecular bands nearer the surface, close to or below $\log \tau_{Ross} = -2$, regions where the number density of H^- is strongly impacted by the magnesium abundance. It is thus particularly important to determine the Mg abundance before computing the molecular lines of C_2 and CN.

As a consequence, in a second step we computed an ATLAS12 model (Kurucz 2005) with these peculiar overabundances of C, N, and Mg, and we iterated to determine the abundances of the different elements. We note that after the NLTE correction, there is a good agreement between the Ca abundance deduced from the Ca I and the Ca II lines (Table 2) confirming the choice of the gravity. The parameters of the model we finally used for the analysis of Pisces II 10694 are: $T_{eff} = 4130$ K, $\log g = 0.8$, $v_t = 2.0$ km s^{-1}, [M/H] = −2.5, A(C) = 7.0, A(N) = 7.0 and A(Mg) = 6.6.

The abundance analysis was performed using the LTE spectral line analysis code `turbospectrum` (Alvarez & Plez 1998; Plez 2012). Since the resolution of the spectra is not very high and since there are many molecular lines all along the spectrum, the lines of the atomic elements are often blended. As a consequence we determined the abundances by fitting synthetic spectra to all visible lines. The results of these computations and the main characteristics of these lines are given in the Appendix (Table A.1). The hyperfine structure has been taken into account, in particular for the Ba II lines.

Table 2. Mean abundance of the elements in the Sun, in Pisces II 10694, the number of lines used for this determination, standard error, $[X/H] = A(X)_\star - A(X)_\odot$, and $[X/Fe] = [X/H]_\star - [Fe/H]_\star$.

Element	$A(X)_\odot$	$A(X)_\star$	N	err	[X/H]	[X/Fe]
Li		≤0.2				
C (CH)	8.50	6.98	–	–	−1.52	+1.08
C (C_2)	8.50	7.28	–	–	−1.23	+1.38
N (CN)	7.86	7.09	–	–	−0.77	+1.81
[O I]	8.76	8.43	2	0.18	−0.33	+2.25
Na I	6.30	4.73	1	–	−1.57	+1.03
Mg I	7.54	6.56	7	0.28	−0.98	+1.60
Ca I	6.33	3.88	7	0.23	−2.45	+0.13
Ca II[a]	6.33	3.94	3	0.19	−2.37	+0.21
Ti I	4.90	2.74	1	–	−2.16	+0.42
Fe I	7.52	4.92	15	0.10	−2.60	–
Ni I	6.23	3.83	2	0.23	−2.40	+0.20
Sr II	2.92	0.5:	2	–	−2.42:	+0.18:
Ba II	2.18	−1.52	3	0.18	−3.70	−1.10

Notes. The solar abundances are from Lodders et al. (2009) for all elements except Fe and C, which are from Caffau et al. (2011a). [(a)] Abundance corrected from non-LTE effects (see text).

The abundance of sodium is deduced from the Na D lines (Table A.1) which are known to present a very strong non-LTE effect in cool metal-poor giants (Andrievsky et al. 2007). However, following Mashonkina et al. (2000), at [Fe/H] = −2 this effect is maximum around $T_{eff} = 5000$ K and decreases very rapidly when the temperature decreases. At $T_{eff} \approx 4100$ K and $\log g \approx 1.0$, (as in Pisces II 10694), the NLTE correction is negligible.

The mean abundances are given in Table 2. Since the red Ca II lines present a very strong non-LTE effect in cool giants, we adopted in Table 2 a correction of −0.3 dex for the red Ca II triplet (based on Spite et al. 2012).

3.1. Abundance of the light elements: Li, C, N, and O

We tried to measure Li in Pisces II 10694. A χ-squared fitting gives A(Li) = 0.0 dex, but in a conservative way we estimated that A(Li) ≤ +0.2 dex.

The abundance of C and N is deduced from the molecular bands of CH, C_2, and CN. The data of these molecular lines are taken from Plez et al. (2008) and Plez (2018). In Fig. 2, as an example, we show the fit of a part of the CH and the C_2 bands. We adopted for the C abundance the mean of the abundances deduced from the CH and the C_2 lines: A(C) = 7.13 (see Tables 2 and A.1). The resolution of the spectrum is not sufficient to determine the ratio $^{12}C/^{13}C$.

The forbidden oxygen lines at 630.03 and 636.38 nm are blended by telluric bands of O_2 and H_2O. The lines of these bands are always weak in our spectra; however, we accounted for them by dividing each of the observed spectra by the corresponding spectrum of the telluric lines[2] (Bertaux et al. 2012, 2014) computed at the time of the observation and at the position of the star. The individual spectra free from telluric lines are then added. The results of these computations are shown in Fig. 3.

[2] http://cds-espri.ipsl.fr/tapas/

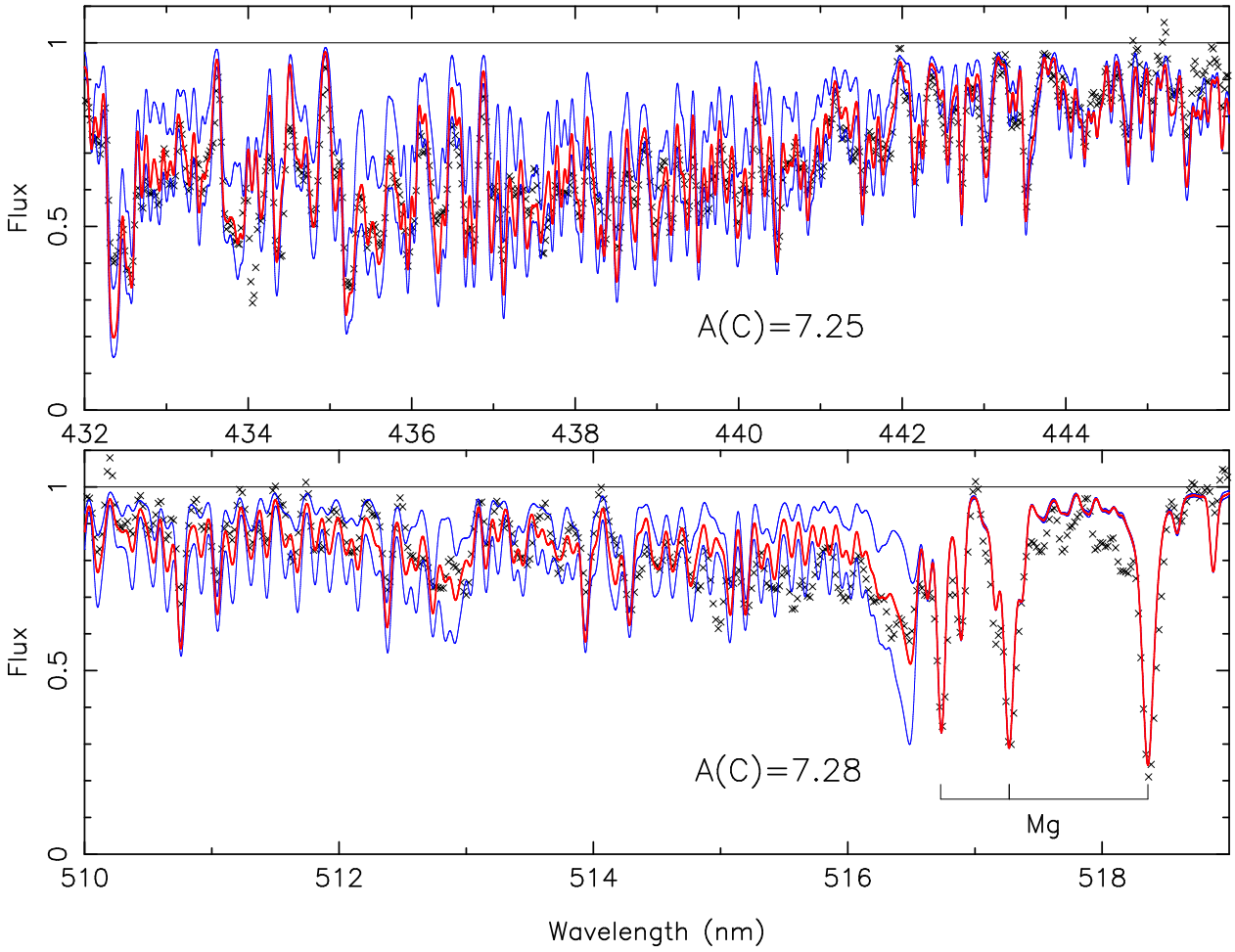

Fig. 2. Spectrum (black crosses) and synthetic profiles of the CH and C_2 bands computed with A(C) = 6.8 and 7.4 for the CH band, and A(C) = 7.1 and A(C) = 7.4 for the C_2 band (blue lines). The red line represents the synthetic spectrum computed with the adopted value of the C abundance in this region of the spectrum (A(C) = 7.28 for the C_2 band and 7.25 for this region of the CH band; see Table A.1). The abscissa is the wavelength in nm. Shown on the red side of the C_2 band is the good fit of the Mg triplet obtained with A(Mg) = 6.6.

In Fig. 4 we compare the C, N, and O abundances in Pisces II 10694 and in carbon-normal metal-poor stars studied homogeneously in the frame of the ESO Large Programme "First Stars" (Spite et al. 2005, 2006; Bonifacio et al. 2009). We added also a classical carbon-rich very metal-poor giant studied in the frame of this Large Programme: CS 2249-37 (Depagne et al. 2002). Mixing processes explain the large scatter observed in the C and N abundances of the carbon-normal metal-poor stars. In giant stars, at different levels of the evolution, mixing occurs between the deep layers and the atmosphere, bringing to the surface CNO processed material: the C abundance decreases and the N abundance increases, but [O/Fe] remains constant. From their atmospheric parameters, Pisces II 10694 and CS 22949-37 are both mixed giants and should be compared to the mixed giants in Fig. 4 (black triangles). Both stars appear to be very enhanced in C, N, and O, and the enhancements are similar.

3.2. Abundance of the neutron-capture elements

On the spectra of Pisces II 10694 we could only measure the Sr and Ba abundances. Only two Sr lines are visible: one (at 407.76 nm) is very blended in a region where the S/N of the UVB spectrum is low; the other line (at 1003.66 nm) is located at the

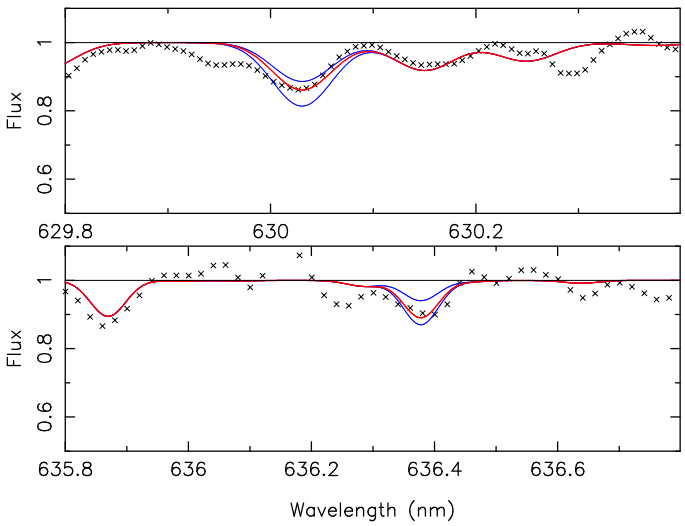

Fig. 3. Fit of the profile of the forbidden oxygen lines. The abscissa is the wavelength in nm. The blue lines show the synthetic spectra computed with A(O) = 8.1 and A(O) = 8.7. The red line is the best fit obtained with A(O) = 8.3 for the line at 630 nm, and A(O) = 8.55 for the line at 636.3 nm.

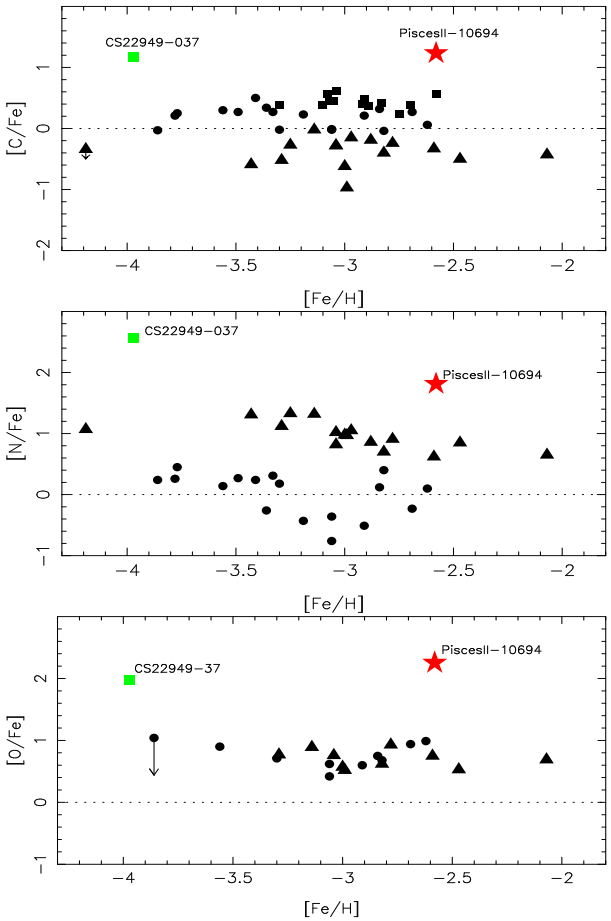

Fig. 4. [C/Fe], [N/Fe], and [O/Fe] vs. [Fe/H] for Pisces II 10694 and a sample of normal galactic very metal-poor stars. The dwarfs are represented by solid squares, the stars in the lower RGB branch by solid circles, and the mixed stars by triangles. The classical galactic CEMP-no giant CS 22949-037 is added (green square). The star Pisces II 10694 is represented by a red star. The large overabundances of C, N, and O in Pisces II 10694 are very similar to those observed in CS 22949-37.

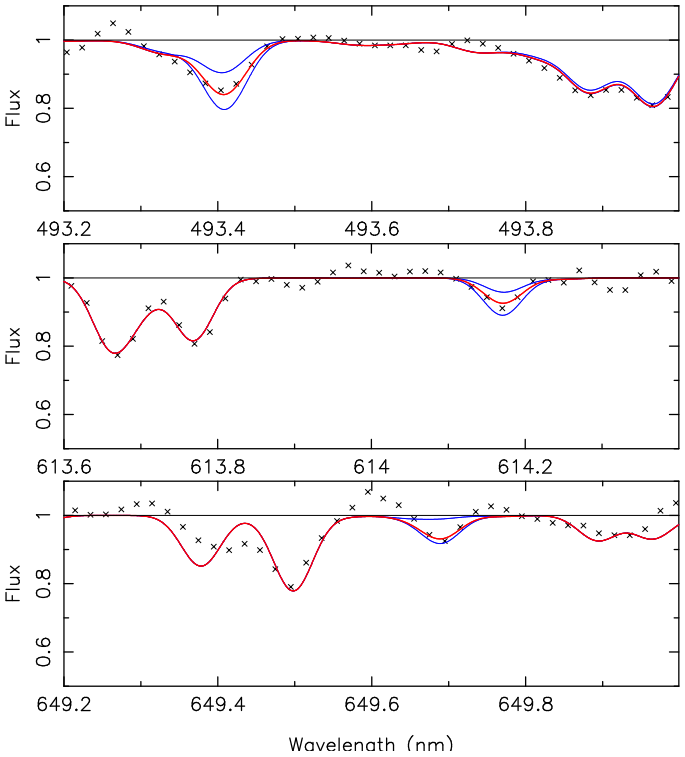

Fig. 5. Fit of the profile of the Ba lines. The abscissa is the wavelength in nm. The blue lines show the synthetic spectrum computed with A(Ba) = −2.4 and A(Ba) = −1.2. The red line is the best fit obtained with A(Ba) = −1.66 for the line at 493.4 nm, A(Ba) = −1.58 for the line at 614.1 nm, and −1.31 for the line at 649.6 nm.

very end of the VIS spectrum. In both cases the measurement of the abundance is very uncertain and we have estimated that the error of [Sr/Fe] is close to 0.5 dex.

We were able to measure four Ba lines. The resonance line of Ba II (at 455.4 nm) is in a very crowded region of the spectrum with a rather low S/N; its measurement is very uncertain, and thus we have determined the abundance of Ba only from the other three lines (Table A.1 and Fig. 5).

4. Discussion

Kirby et al. (2015) consider that Pisces II 10694 belongs to the UFD galaxy Pisces II, mainly from the radial velocity of the star. With the *Gaia* Data Release 2 (DR2; Gaia Collaboration 2016, 2018a; Arenou et al. 2018), it is possible in some Local Group galaxies to use the proper motions and even the parallaxes of the stars to confirm that they are true members (e.g. Gaia Collaboration 2018b; Simon 2018; Fritz et al. 2018). At present this is not possible for Pisces II because these quantities are now available for only two spectroscopic members of Pisces II (9004 and 10694). They have been used to infer a systemic proper motion for the system (Fritz et al. 2018), but the large uncertainty of the parallaxes and proper motions hamper the possibility of safely identifying them as possible foreground stars.

4.1. The CEMP type of Pisces II 10694

4.1.1. Abundance of C, N, O

In Fig. 6 we have plotted the abundance of C versus [Fe/H] for galactic metal-poor turn-off stars (Spite et al. 2013; Bonifacio et al. 2015). In turn-off stars, the original C abundance is not diluted by mixing with deep layers where C is transformed into N, and thus the C abundance measured in these stars is expected to be the abundance of carbon in the cloud from which the star formed. The "normal" metal-poor turn-off stars like those studied in Bonifacio et al. (2015) in the frame of the ESO Large Programme "First Stars" from high-resolution, high S/N spectra are located in the grey zone of the figure. Their relatively high C abundance (measured from the CH band): ([C/Fe] = +0.45 ± 0.10) is in agreement with the models of the chemical evolution of the Galaxy (see e.g. Romano et al. 2010). We thus adopted [C/Fe] ≥ +1 as a definition of the C-rich stars to avoid the tail of the distribution of the normal metal-poor stars as already proposed by Beers & Christlieb (2005).

With this definition of the C-rich stars, the carbon-rich turn-off stars, in Fig. 6 are located inside two different bands (Spite et al. 2013; Bonifacio et al. 2015).

Most of the stars in the highest carbon band are Ba-rich and sometimes also Pb-rich; however, some rare stars have been found to be CEMP-no.

On the contrary, all the stars in the lowest hatched blue C band have been found to be CEMP-no (see Fig. 6 in

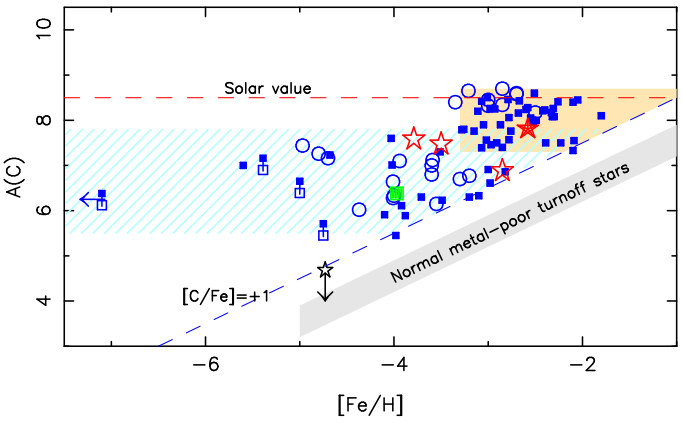

Fig. 6. Abundance of carbon A(C) vs. [Fe/H] in dwarfs and turn-off galactic CEMP stars from the literature (blue squares). Only the determinations obtained from high-resolution spectra were selected. The measurements made homogeneously by our team are represented with open blue circles. The dashed blue line (representing [C/Fe] = +1) separates the region of the carbon-rich metal-poor stars from the region of the normal metal-poor stars. On the upper A(C) band (yellow zone) all the stars but four are Ba-rich. On the contrary, on the lower A(C) band (hatched blue zone) all the stars are CEMP-no. Below [Fe/H] = −3.4 all the CEMP stars belong to the second group. The Pisces II 10694 star is represented by a red filled star and the CEMP giants in the dwarf galaxies Sculptor, Boo I and Seg I, by open red stars. The galactic giant CS 22949-037 is represented by a filled green square.

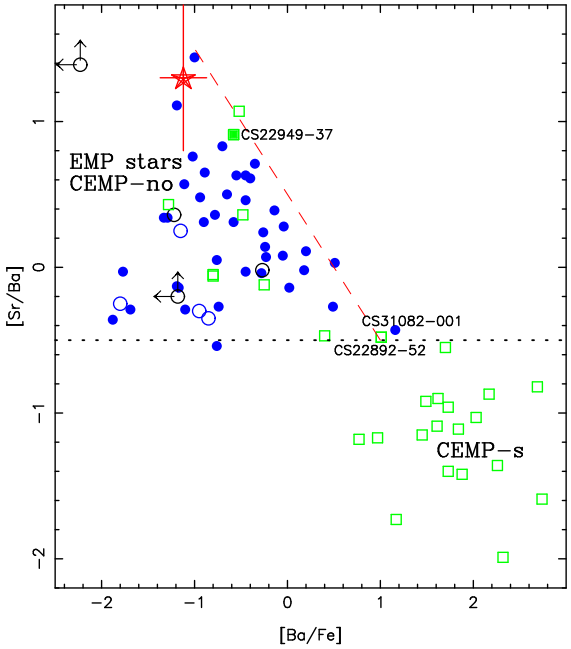

Fig. 7. [Sr/Ba] vs. [Ba/Fe] in normal very metal-poor stars in our Galaxy (blue filled circles), in the stars in the dwarf galaxy Sculptor (black open circles), and in Tuc II (blue open circles). The green open squares represent a sample of Galactic CEMP stars studied from high-resolution spectra. The black dotted line at [Sr/Ba] ≈ −0.5 represents the pure *r*-process production as observed for example in the EMP star CS 31082-001 (Cayrel et al. 2001; Hill et al. 2002) and the CEMP star CS 22892-52 (Sneden et al. 2000, 2003). The CEMP stars with a high value of [Ba/Fe] and a low value of [Sr/Ba] have been enriched in neutron-capture elements by the ejecta of an AGB. Many CEMP stars have the same range of [Sr/Ba] as the normal EMP stars. They are CEMP-no. The red star represents Pisces II 10694. It is very similar to the galactic C-rich giant CS 22949-037 (filled green square).

Bonifacio et al. 2015, for more details). Below [Fe/H] = −3.4 all the CEMP stars belong to this second group.

It is generally considered that the CEMP-no stars were born with the observed chemical composition. On the contrary, the chemical composition of the CEMP-s stars is explained by a mass-transfer from a companion in its asymptotic giant branch (AGB) phase. Most of the CEMP-s stars show radial velocity variations, which suggests that they are all binaries (Lucatello et al. 2005; Starkenburg et al. 2014).

If we want to compare the C, N, O abundances in stars of our Galaxy and in the carbon-rich Pisces II 10694, we have to take into account that it is not a turn-off star and that extra mixing could occur, inducing a transformation of C into N and thus a decrease in the C abundance. In Fig. 4 (upper panel) the difference in [C/Fe] between turn-off stars and evolved mixed giants is about +0.7 dex (see also Spite et al. 2005, 2006; Bonifacio et al. 2009). In the same way, in Fig. 4 (middle panel) we estimate that the correction for [N/Fe] is about −0.8 dex.

In Fig. 6 we have added the position of Pisces II 10694 (filled red star symbol) and as a comparison, the position of the classical galactic evolved C-rich giant CS 22949-037 Depagne et al. (2002). Both stars are cool giants with $\log g = 0.8$ and 1.5 dex and their C abundance has to be corrected for extra mixing. We adopted the same correction for these two stars (+0.7 dex).

Two CEMP stars have been identified in the dwarf galaxy Sculptor (Skúladóttir et al. 2015; Chiti et al. 2018), but following our definition of the C-rich stars, only one can be considered a CEMP: Sculptor 11-1-4422 with [C/Fe] = 1.26 dex, after mixing correction. In the UFD galaxy Bootes I, Lai et al. (2011) measured for Boo21 [C/Fe] = +2.20, or [C/Fe] = +2.90 after mixing correction. This star is also known as Boo-119 (Gilmore et al. 2013; Frebel et al. 2016). In the UFD galaxy Segue I, a CEMP star has been also detected: Segue I-7 with [C/Fe] = +2.30, or [C/Fe] = +2.50 after mixing correction (Norris et al. 2010b). These stars have been also plotted in Fig. 6. The stars Sculptor 11-1-4422, Boo-119, and Segue I-7 clearly belong to the lower A(C) band where all the stars are CEMP-no. The star Pisces II 10694 with its higher metallicity, is located at the limit between the lower and the higher A(C) band.

The oxygen abundance is also very high in Pisces II 10694: [O/Fe] = +2.25 (in normal EMP stars indeed, the oxygen abundance at this metallicity is close to [O/Fe] = +0.7). This strong enhancement is close to that observed in the galactic CEMP star CS 22949-37: [O/Fe] = +1.98 (Depagne et al. 2002).

4.1.2. Neutron-capture elements

As said previously, Pisces II 10694 is not Ba-rich and thus it is a CEMP-no star. Since we were able to obtain an estimation of the Sr abundance in this star (Table 2), it is interesting to check whether it shares the same characteristics as the other CEMP-no stars.

In Fig. 7 we have plotted [Sr/Ba] versus [Ba/Fe] for a sample of normal galactic metal-poor stars studied in the frame of the ESO Large Programme "First Stars". All these stars are located in a well-defined region of this diagram (see e.g. Spite et al. 2018). Many Galactic CEMP stars are found in the same region as the normal EMP stars. They are CEMP-no with [Sr/Ba] > −0.5. The limit [Sr/Ba] ≈ −0.5 corresponds to the production of a pure *r*-process (dotted line on Fig.7).

On the other hand, in our Galaxy many CEMP stars are extremely rich in Ba ([Ba/Fe] > 1) and their ratio [Sr/Ba] is lower than the *r*-process limit. These stars have likely been enriched by the ejecta of AGB stars or super-AGB stars forming neutron-capture elements through the *s*-process (e.g. Busso et al. 1999) or the *i*-process (e.g. Hampel et al. 2016, and references therein).

Jablonka et al. (2015) measure the abundance of Sr and Ba in stars of the dwarf galaxy Sculptor. In Fig. 7 we compare the ratio [Sr/Ba] in the normal metal-poor stars in Sculptor and in our Galaxy; the stars of both galaxies occupy the same region of the diagram suggesting a similar origin for these elements. Unfortunately Chiti et al. (2018) were not able to measure the abundance of Ba and Sr in the C-rich star Sculptor 11-1-4422, and thus we do not plot this star in Fig. 7.

Since the Pisces II stars are very faint, there is no determination of the abundance of the neutron-capture elements in these stars other than Pisces II 10694. The position of Pisces II 10694 in Fig. 7 suggests that it is a classical CEMP-no star, as is CS 22949-037 in our Galaxy. The position of Pisces II 10694 in this diagram is also very close to the position of the normal very metal-poor giant HD 122563, and it would be interesting to compare the neutron-capture element pattern in Pisces II 10694 and in HD 122563. This will certainly be possible when a high-resolution spectrograph is available on the next generation of extremely large telescopes, but it may also be within reach of ESPRESSO (Pepe et al. 2013, 2014) fed by the four VLT telescopes.

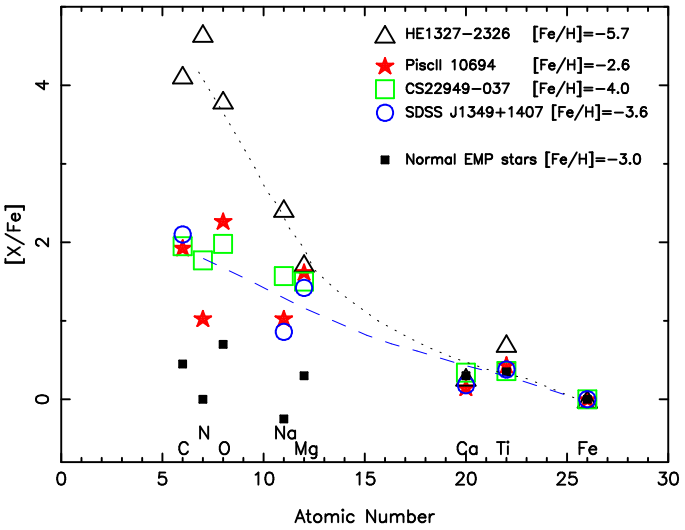

Fig. 8. Abundance pattern of the elements in Pisces II 10694 and three other galactic C-rich stars with [Fe/H] = −3.6, −4.0 and −5.7. The abundance pattern of the elements in Pisces II 10694 is very similar to the pattern observed in CS 22949-037 and SDSS J1349+1407. In HE 1327-2326 which has an extremely low metal abundance, the enhancement of C, N, O, Na is stronger and the decrease steeper. In all the stars the abundance of the elements from Ca and heavier is normal. The dashed blue line shows the mean abundance pattern of the elements in Pisces II 10694, CS 22949-037, and SDSS J1349+1407, and the dotted grey line the mean abundance pattern in HE 1327-2326.

4.2. Chemical imprint by the first stars

The existence of a CEMP-no star in the UFD galaxy Pisces II (with $L \sim 10^4\ L_\odot$) is consistent with theoretical predictions of cosmological models (e.g. Salvadori et al. 2015) and hydro-dynamical simulations (e.g. Jeon et al. 2017) suggesting that these small galaxies might be the living relics of star-forming mini-halos hosting the first stars. In these studies, long-lived CEMP-no stars form in gaseous environments predominantly imprinted by the chemical products of primordial low-energy faint supernovae (SNe; e.g. Bonifacio et al. 2003; Nomoto et al. 2003). The observed [C/Fe] = +1.23 and [Fe/H] = −2.6 of Pisces II 10694 suggest that its birth environment was likely polluted by both primordial faint SNe and normal Pop II stars exploding as core-collapse supernovae (Salvadori et al. 2015 section 4, and also de Bennassuti et al. 2017).

Salvadori et al. (2015) investigated the frequency of CEMP-no stars in dwarf galaxies with different luminosities. One of their key results is that the probability of observing CEMP-no stars, imprinted by primordial faint SNe, increases with decreasing galaxy luminosity and, on average, this probability is an order of magnitude higher in UFDs than in more massive classical Sculptor-like dwarf spheroidal galaxies. This is a direct consequence of the association between UFDs and low-mass mini-halos. The detection of a single CEMP-no star in Pisces II do not allow us to make statistical comparisons with model predictions. However, our observational confirmation of one CEMP-no star out of the four stars identified by Kirby et al. (2015) at [Fe/H] < −2 supports the idea that the probability of observing CEMP-no stars is high in ultra-faint dwarf galaxies.

5. Conclusion

In Pisces II only seven stars have been spectroscopically observed (Kirby et al. 2015), and one of these stars Pisces II 10694, was found to be very metal-poor and was suspected to be C-rich.

– We confirmed (Fig. 4) that Pisces II 10694 is a CEMP star. Its low lithium abundance (A(Li) < +0.2 dex) suggests that this cool giant star has undergone some extra mixing. As a consequence we adopted a correction of +0.7 dex for [C/Fe] and −0.8 dex for [N/Fe].

– The ratios [N/Fe], [O/Fe], [Na/Fe], and [Mg/Fe] are also strongly enhanced in Pisces II 10694. The abundances of Ca to Ni are normal compared to the classical (not C-rich) EMP stars. The abundances of the α elements Mg, Ca, and Ti are only slightly enhanced relative to Fe, as is generally observed in metal-poor stars.

– The abundance pattern in Pisces II 10694 (Fig. 8) is similar to that observed in the galactic C-rich giant CS 22949-037 (Depagne et al. 2002), and in SDSS J1349+1407, a turn-off CEMP star recently reported by Bonifacio et al. (2018). These three stars have a metallicity [Fe/H] between −2.6 and −4.0.

In Fig. 8 we have also added the abundance pattern of the galactic extremely metal-poor C-rich subgiant HE1327-2326: [Fe/H] = −5.7 following Frebel et al. (2008). In this star, the enhancement of C, N, O, and Na is much stronger, but the decrease of this enhancement with the atomic number is steeper. All the stars in Fig. 8 have a normal [Ca/Fe] ratio.

– The carbon abundance in Pisces II 10694 (A(C) = 7.73 with the extra-mixing correction) put this star at the limit between the lower and the higher A(C) band (Fig. 6 and Spite et al. 2013; Bonifacio et al. 2015).

– The observed chemical properties of Pisces II 10694 suggest that it is a CEMP-no star. The abundance of strontium and barium are very low in Pisces II 10694, as they are in the classical Galactic CEMP-no star CS 22949-037. Our observational confirmation of a CEMP-no star in the UFD galaxy Pisces II agrees with the predictions of theoretical models that follow early

cosmic star formation in low-mass mini-halos and trace the chemical signature of zero-metallicity stars exploding as faint SN (e.g. Salvadori et al. 2015). Hence, our results suggest that the UFD galaxy Pisces II might be the living fossil of a star-forming mini-halo hosting the first stars. To make statistical comparisons between model predictions and observations of UFD galaxies, larger samples of CEMP-no stars are required. Our observational findings show that the Pisces II galaxy is a perfect place to look for more iron-poor, highly C-enhanced CEMP-no stars similar to those found in the Galactic halo and in the faintest UFD Segue I.

Acknowledgements. This work has made use of data from the European Space Agency (ESA) mission *Gaia* (https://www.cosmos.esa.int/gaia), processed by the *Gaia* Data Processing and Analysis Consortium (DPAC, https://www.cosmos.esa.int/web/gaia/dpac/consortium). Funding for the DPAC has been provided by national institutions, in particular the institutions participating in the *Gaia* Multilateral Agreement. Stefania Salvadori is supported by the Italian Ministry of Education, University, and Research (MIUR) through a Rita Levi Montalcini Fellowship.

References

Abate, C., Pols, O. R., Stancliffe, R. J., et al. 2015, A&A, 581, A62
Allen, D. M., Ryan, S. G., Rossi, S., Beers, T. C., & Tsangarides, S. A. 2012, A&A, 548, A34
Alvarez, R., Plez, B., 1998, A&A 330, 1109
Andrievsky, S. M., Spite, M., Korotin, S. A., et al. 2007, A&A, 464, 1081
Arenou, F., Luri, X., Babusiaux, C., et al. 2018, A&A, 616, A17
Beers, T. C. 2018, Am. Astron. Soc. Meet. Abstr., 232, 114.05
Beers, T. C., & Christlieb, N. 2005, Highlights of Astronomy, 13, 579
Belokurov, V., Walker, M. G., Evans, N. W., et al. 2010, ApJ, 712, L103
Bertaux, J. L., Lallement, R., Ferron, S., et al. 2012, TAPAS: a web-based service of atmospheric transmission computation for astronomy, ASA/HITRAN Conf.
Bertaux, J. L., Lallement, R., Ferron, S., et al. 2014, A&A 564, A46
Bonifacio, P., Limongi, M., & Chieffi, A. 2003, Nature, 422, 834
Bonifacio, P., Spite, M., Cayrel, R., et al. 2009, A&A, 501, 519
Bonifacio, P., Caffau, E., Spite, M., et al. 2015, A&A, 579, A28
Bonifacio, P., Caffau, E., Spite, M., et al. 2018, A&A, 612, A65
Bovill, M. S., & Ricotti, M. 2009, ApJ, 693, 1859
Busso, M., Gallino, R., & Wasserburg, G. J. 1999, ARA&A, 37, 239
Caffau, E., Bonifacio, P., François, P., et al. 2011a, Nature, 477, 67
Caffau, E., Ludwig, H.-G., Steffen, M., Freytag, B., & Bonifacio, P. 2011b, Sol. Phys., 268, 255
Caffau, E., Bonifacio, P., François, P., et al. 2013, A&A, 560, A15
Caffau, E., Gallagher, A. J., Bonifacio, P., et al. 2018, A&A, 614, A68
Cayrel, R., Hill, V., Beers, T. C., et al. 2001, Nature, 409, 691
Cayrel, R., Depagne, E., Spite, M., et al. 2004, A&A, 416, 1117
Chiti, A., Simon, J. D., Frebel, A., et al. 2018, ApJ, 856, 142
Cooke, R. J., & Madau, P. 2014, ApJ, 791, 116
de Bennassuti, M., Schneider, R., Valiante, R., & Salvadori, S. 2014, MNRAS, 445, 3039
de Bennassuti, M., Salvadori, S., Schneider, R., Valiante, R., & Omukai, K. 2017, MNRAS, 465, 926
Demarque, P., Woo, J.-H., Kim, Y.-C., & Yi, S. K. 2004, ApJS, 155, 667
Denissenkov, P. A., & Pinsonneault, M. 2008, ApJ, 679, 1541
Depagne, E., Hill, V., Spite, M., et al. 2002, A&A, 390, 187
D´Odorico, S., Dekker, H., Mazzoleni, R., et al. 2006, Proc. SPIE, 6269, 98
François, P., Depagne, E., Hill, V., et al. 2007, A&A, 476, 935
François, P., Monaco, L., Bonifacio, P., et al. 2016, A&A, 588, A7
Frebel, A., Collet, R., Eriksson, K., Christlieb, N., & Aoki, W. 2008, ApJ, 684, 588
Frebel, A., Simon, J. D., & Kirby, E. N. 2014, ApJ, 786, 74
Frebel, A., Chiti, A., Ji, A. P., Jacobson, H. R., & Placco, V. M. 2015, ApJ, 810, L27
Frebel, A., Norris, J. E., Gilmore, G., & Wyse, R. F. G. 2016, ApJ, 826, 110
Fritz, T. K., Battaglia, G., Pawlowski, M. S., et al. 2018, A&A, submitted [arXiv: 1805.00908]
Gaia Collaboration (Prusti, T., et al.) 2016, A&A, 595, A1
Gaia Collaboration (Brown, A. G. A., et al.) 2018a, A&A, 616, A1
Gaia Collaboration (Helmi, A., et al.) 2018b, A&A, 616, A12
Gilmore, G., Norris, J. E., Monaco, L., et al. 2013, ApJ, 763, 61
Guinouard, I., Horville, D., Puech, M., et al. 2006, Proc. SPIE, 6273, 62733R
Gustafsson, B., Bell, R. A., Eriksson, K., & Nordlund, Å., 1975, A&A, 42, 407
Gustafsson, B., Edvardsson, B., Eriksson, K., et al. 2003, in Stellar Atmosphere Modeling, eds. I. Hubeny, D. Mihalas, & K. Werner, ASP Conf. Ser., 288, 331
Gustafsson, B., Edvardsson, B., Eriksson, K., et al. 2008, A&A, 486, 951
Hampel, M., Stancliffe, R. J., Lugaro, M., & Meyer, B. S. 2016, ApJ, 831, 171
Hansen, C. J., Nordström, B., Hansen, T. T., et al. 2016, A&A, 588, A37
Hill, V., Plez, B., Cayrel, R., et al. 2002, A&A, 387, 560
Jablonka, P., North, P., Mashonkina, L., et al. 2015, A&A, 583, A67
Jeon, M., Besla, G., & Bromm, V. 2017, ApJ, 848, 85
Ji, A. P., Frebel, A., Simon, J. D., & Chiti, A. 2016a, ApJ, 830, 93
Ji, A. P., Frebel, A., Ezzeddine, R., & Casey, A. R. 2016b, ApJ, 832, L3
Kirby, E. N., Simon, J. D., Geha, M., Guhathakurta, P., & Frebel, A. 2008, ApJ, 685, L43
Kirby, E. N., Simon, J. D., & Cohen, J. G. 2015, ApJ, 810, 56
Kurucz, R. L. 2005, Mem. Soc. Astron. It. Suppl., 8, 14
Lai, D. K., Lee, Y. S., Bolte, M., et al. 2011, ApJ, 738, 51
Lee, Y. S., Beers, T. C., Masseron, T., et al. 2013, AJ, 146, 132
Lee, Y. S., Suda, T., Beers, T. C., & Stancliffe, R. J. 2014, ApJ, 788, 131
Lodders, K., Plame, H., Gail, H.-P. 2009, Landolt-Börnstein – Group VI Astronomy and Astrophysics Numerical Data and Functional Relationships in Science and Technology, ed. J.E. Trümper, 4.4, 44
Lucatello, S., Tsangarides, S., Beers, T. C., et al., 2005, ApJ, 625, 825
Mashonkina, L. I., Shimanskiĭ, V. V., & Sakhibullin, N. A. 2000, Astron. Rep., 44, 790
Masseron, T., Johnson, J. A., Plez, B., et al. 2010, A&A, 509, A93
McWilliam, A., Preston, G. W., Sneden, C., & Searle, L. 1995, AJ, 109, 2757
Nomoto, K., Umeda, H., Maeda, K., et al. 2003, Nucl. Phys. A, 718, 277
Norris, J. E., Ryan, S. G., & Beers, T. C. 2001, ApJ, 561, 1034
Norris, J. E., Gilmore, G., Wyse, R. F. G., Yong, D., & Frebel, A. 2010a, ApJ, 722, L104
Norris, J. E., Wyse, R. F. G., Gilmore, G., et al. 2010b, ApJ, 723, 1632
Pepe, F., Cristiani, S., Rebolo, R., et al. 2013, The Messenger, 153, 6
Pepe, F., Molaro, P., Cristiani, S., et al. 2014, Astron. Nachr., 335, 8
Plez, B., 2012, Astrophysics Source Code Library [record ascl:1205.004]
Plez, B., 2018, https://nextcloud.lupm.univ-montp2.fr/s/r8pXijD39YLzw5T
Plez, B., Masseron, T., Van Eck, S., et al. 2008, in 14th Cambridge Workshop on Cool Star, Stellar Systems, and the Sun, ed. G. van Belle, ASP Conf Ser., 384, CD-Rom
Romano, D., Karakas, A. I., Tosi, M., & Matteucci, F. 2010, A&A, 522, A32
Salvadori, S., & Ferrara, A. 2009, MNRAS, 395, L6
Salvadori, S., Skúladóttir, Á., & Tolstoy, E. 2015, MNRAS, 454, 1320
Simon, J. D. 2018, ApJ, 863, 89
Skúladóttir, Á., Tolstoy, E., Salvadori, S., et al. 2015, A&A, 574, A129
Sneden, C., McWilliam, A., Preston, G. W., et al. 1996, ApJ, 467, 819
Sneden, C., Cowan, J. J., Ivans, I. I., et al. 2000, ApJ, 533, L139
Sneden, C., Cowan, J. J., Lawler, J. E., et al. 2003, ApJ, 591, 936
Spite, M., Cayrel, R., Plez, B., et al. 2005, A&A, 430, 655
Spite, M., Cayrel, R., Hill, V., et al. 2006, A&A, 455, 291
Spite, M., Andrievsky, S. M., Spite, F., et al. 2012, A&A, 541, A143
Spite, M., Caffau, E., Bonifacio, P., et al. 2013, A&A, 552, A107
Spite, F., Spite, M., Barbuy, B., et al. 2018, A&A, 611, A30
Starkenburg, E., Shetrone, M. D., McConnachie, A. W., & Venn, K. A. 2014, MNRAS, 441, 1217
Vernet, J., Dekker, H., D´Odorico, S., et al. 2011, A&A, 536, A105
Yoon, J., Beers, T. C., Placco, V. M., et al. 2016, ApJ, 833, 20

Appendix A

Table A.1. LTE determination of the abundance $A(X) = \log(N_X/N_H) + 12$ of the elements in Pisces II 10694.

Element	wavelength in Å	χ_{ex}	$\log gf$	A(X)	Element	wavelength in Å	χ_{ex}	$\log gf$	A(X)
C (CH)	4260-4300	–	–	6.68	Ca II	8498.1	1.69	−1.429	4.46
C (CH)	4294-4316	–	–	6.74	Ca II	8542.1	1.70	−0.463	4.11
C (CH)	4320-4340	–	–	7.28	Ca II	8662.2	1.69	−0.723	4.15
C (CH)	4360-4380	–	–	7.23					
					Ti I	6258.1	1.44	−0.390	2.74
C (C_2)	5030-5140	–	–	7.24	Ti I	6258.7	1.46	−0.280	2.74
C (C_2)	5120-5165	–	–	7.31					
					Fe I	6065.5	2.61	−1.530	5.04
N (CN)	4120-4200	–	–	6.73	Fe I	6136.6	2.45	−1.400	4.94
N (CN)	4200-4215	–	–	6.88	Fe I	6137.7	2.59	−1.403	4.94
N (CN)	8070-8350	–	–	7.35	Fe I	6191.6	2.43	−1.417	4.88
N (CN)	8308-8350	–	–	7.09	Fe I	6213.4	2.22	−2.482	5.00
N (CN)	8362-8388	–	–	7.06	Fe I	6219.3	2.20	−2.433	4.94
N (CN)K[a]	8308-8350	–	–	7.15	Fe I	6230.7	2.56	−1.281	4.89
N (CN)K[a]	8362-8388	–	–	7.36	Fe I	6252.6	2.40	−1.687	4.97
					Fe I	6256.4	2.45	−2.408	4.97
[O I]	6300.3	0.00	−9.78	8.30	Fe I	6265.1	2.18	−2.550	4.82
[O I]	6363.8	0.00	−10.258	8.55	Fe I	6393.6	2.43	−1.432	4.83
					Fe I	6400.0	3.60	−0.290	4.70
Na I	5890.0	0.00	−0.194	4.73	Fe I	6421.4	2.28	−2.027	4.84
					Fe I	6430.9	2.18	−2.006	4.86
Mg I	4703.0	4.35	−0.440	6.32	Fe I	6678.0	2.69	−1.418	5.13
Mg I	5167.3	2.71	−0.931	6.68					
Mg I	5172.7	2.71	−0.450	6.78	Ni I	6643.6	1.68	−2.300	3.99
Mg I	5183.6	2.72	−0.239	6.90	Ni I	6767.8	1.83	−2.170	3.67
Mg I	5528.4	4.35	−0.498	6.11					
Mg I	8717.8	5.93	−0.865	6.70	Sr II	4077.7	0.00	+0.167	0.20:
Mg I	8736.0	5.95	−0.350	6.44	Sr II	10036.7	1.81	−1.312	0.80:
Ca I	5598.5	2.52	−0.087	3.76	Ba II	4554.0	0.00	+0.170	−2.15:
Ca I	5857.4	2.93	+0.240	4.23	Ba II	4934.1	0.00	−0.150	−1.66
Ca I	6102.7	1.88	−0.793	4.06	Ba II	6141.7	0.70	−0.076	−1.58
Ca I	6122.2	1.89	−0.316	3.56	Ba II	6496.9	0.60	−0.377	−1.31
Ca I	6162.2	1.90	−0.090	3.90					
Ca I	6439.1	2.53	+0.390	3.70					
Ca I	6493.8	2.52	−0.109	3.92					

Notes. [(a)] Abundance measured on the Kirby spectrum.